

Transmittivity measurements by means of squeezed vacuum light

V. D'Auria^{\$†}, C. de Lisio^{\$†}, A. Porzio^{\$}, S. Solimeno^{\$†}

^{\$} Coherentia–CNR–INFM

and

[†] Dipartimento di Scienze Fisiche, Univ. “Federico II”
Compl. Univ. Monte Sant’Angelo, 80126 Napoli, Italia

Matteo G.A. Paris

Dipartimento di Fisica dell’Università di Milano, Italia.

Abstract. A method for measuring the transmittivity of optical samples by using squeezed–vacuum radiation is illustrated. A squeezed vacuum field generated by a below–threshold optical parametric oscillator is propagated through a nondispersive medium and detected by a homodyne apparatus. The variance of the detected quadrature is used for measuring the transmittivity. With this method it is drastically reduced the number of photons passing through the sample during the measurement interval. The results of some tests are reported.

1. Introduction

Vacuum fluctuations of electro–magnetic (*e.m.*) fields have been the ultimate limit on the precision of optical measurements until the advent of squeezed light. Since then, many attempts have been made for reducing the shot noise level blurring several types of signals. Caves [1] first proposed to combine coherent and squeezed vacuum radiation for overcoming the quantum limit in gravitational wave antennas. Grangier et al. [2] up-graded a polarization interferometer by injecting a squeezed vacuum through a dark port. Polzik et al. [3] provided stunning evidence that a gain of some dB over the standard quantum limit is achieved in the resonant interaction of atoms with squeezed light. Their experiment was performed by combining in a well defined phase relation a coherent field with the output of an optical parametric oscillator (OPO) operating below–threshold.

Other experiments have exploited the correlation between twin beams for reducing the noise level of the probe field [4, 5, 6, 7]. The principles of these measurements were highlighted in Ref. [4], where it was recognized that the losses occurring in one beam can be inferred from those relative to the other one (see also [6, 7, 8]).

In this communication a method for probing the transmittivity T of a sample with squeezed vacuum radiation is discussed. Standard methods rely on direct measurement

of the radiation intensity entering and leaving the sample. Sufficient accuracy can be achieved by using beams so intense to contrast the shot-noise, although, in some circumstances, using high input intensity is either not useful (in case of very low absorption) or unwise (strongly non-linear materials or samples whose structure may be altered by intense photon fluxes).

In alternative to the above schemes [1, 2, 3] in the proposed method the sample is irradiated with a squeezed vacuum field. Then, the emerging one is combined with a coherent one (local oscillator, LO) in a balanced homodyne detector measuring the fluctuations in a suitable spectral range. The interaction of the squeezed vacuum with the sample modifies the spectrum of the homodyne current by changing its variance. Hence, the transmittivity is determined by measuring the variance changes. The main advantage of this method is a very low number of photons interacting with the sample.

Below-threshold degenerate OPOs produce *e.m.* radiation represented by a combination of squeezed vacuum and thermal components (squeezed-thermal-vacuum states, STV) with a Gaussian statistics. The OPO working conditions determine the STV state properties [9, 10]. The propagation through non resonant media transforms such a state into another STV one with different variances of the field quadratures ΔX_ϕ^2 . The change of ΔX_ϕ^2 is used for measuring the transmittivity T (Section 2).

The squeezed radiation is analyzed by a balanced homodyne detector providing the field quadratures $X_\phi = \frac{1}{2}(ae^{-i\phi} + a^\dagger e^{i\phi})$ via the controlled interference between the STV state and a strong coherent LO of relative phase ϕ . Since the detected signal is proportional to X_ϕ times the LO amplitude, the detection is efficient also in case of very weak beams, as in the present case. Consequently, the effects of the SNR on the accuracy can be disregarded.

Essential to this method is the use of a Gaussian distributed quadrature X_ϕ . This means that for testing the method it is necessary to preliminarily measure the distribution function by sampling X_ϕ an adequate number N of times. In alternative, it is also possible to determine the whole Wigner function with quantum homodyne tomography (QHT) [11] using samples uniformly distributed over the whole interval $(0, 2\pi)$. Distributing N samples in the interval $(0, 2\pi)$ reduces the accuracy of only a few percent. This slight loss is largely compensated by a three dimensional characterization of the STV state in the phase space.

Aim of this communication is to assess the feasibility of this scheme by testing the validity of two main assumptions, namely *i*) the generation of Gaussian STV states by a below-threshold OPO, and *ii*) the description of the absorption process as a simple scaling of the P-representation of the STV state. The dependence of the accuracy of the proposed method on the STV state parameters is also examined. Moreover, the method accuracy is compared with that achievable with standard techniques. Some measurements carried out with a below-threshold type-I Lithium Niobate (LNB) OPO at $\lambda = 1064$ nm, typically generating few pW STV states are illustrated.

The paper is organized as follows. In the next section the properties of the STV states undergoing lossy propagation are discussed. Then, in Section 3, the

accuracy of the measurement of T based on this method is compared with that of different techniques. Section 4 is dedicated to the description of the experimental tests. Eventually, in Section 5, conclusions are drawn.

2. Generation and propagation of STV states

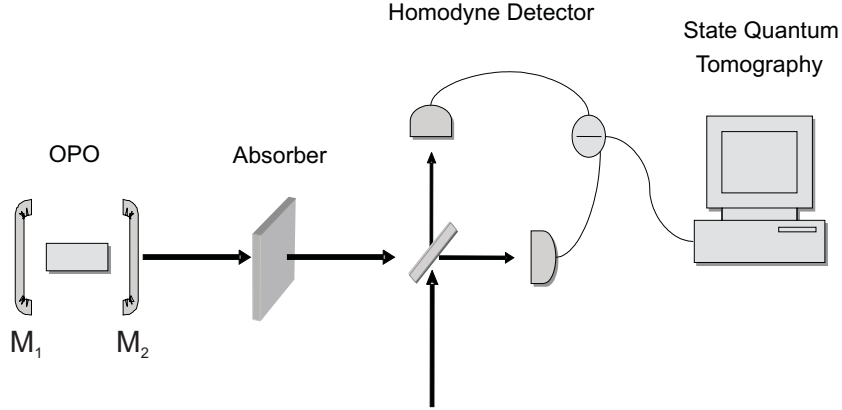


Figure 1. Schematic of the OPO cavity and the experimental setup. The STV states, generated by the OPO, pass through a sample of variable transmittivity T and then are characterized by a homodyne detector. State parameters are recovered by QHT data processing.

The field generated by a below-threshold OPO satisfies the Langevin equation:

$$\frac{d}{dt} \begin{bmatrix} a \\ a^\dagger \end{bmatrix} = (\gamma + \delta\gamma(t)) \begin{bmatrix} a^\dagger \\ a \end{bmatrix} - \begin{bmatrix} (\kappa + i\psi + i\delta\psi(t)) a \\ (\kappa - i\psi - i\delta\psi(t)) a^\dagger \end{bmatrix} + \sqrt{2\kappa_1} \begin{bmatrix} a_1^{in} \\ a_1^{in\dagger} \end{bmatrix} + \sqrt{2\kappa_2} \begin{bmatrix} a_2^{in} \\ a_2^{in\dagger} \end{bmatrix}, \quad (1)$$

where a_1^{in} is the noise entering the cavity through the output mirror M_1 (see Fig. 1) and a_2^{in} represents both the noise entering through the input mirror M_2 and the crystal contribution. The quantities κ_1, κ_2 are damping coefficients, whereas $\kappa = \kappa_1 + \kappa_2$. The parametric gain is the sum of a stationary mean value, γ , and a small fluctuating contribution, $\delta\gamma(t)$. Similarly, ψ and $\delta\psi(t)$ are the mean cavity detuning and its fluctuations, respectively. In this context, the ratio $\mathcal{E} = \gamma^2/\kappa^2$ represents the distance of the actual operating condition from the OPO threshold power, while κ_1/κ is the so called coupling efficiency.

In the frequency domain the variance ΔX^2 of the output quadrature $X = X_{\phi=0}$ reads as:

$$\Delta X^2 = \frac{|\kappa^2 - \gamma^2 - (\omega^2 - \psi^2) + i2\omega\kappa - 2\kappa_1(\kappa + i(\omega - \psi) + \gamma)|^2 + 4\kappa_1\kappa_2|\kappa + i(\omega - \psi) + \gamma|^2}{4|\kappa^2 - \gamma^2 - (\omega^2 - \psi^2) + i2\omega\kappa|^2} \quad (2)$$

where ω is the frequency offset from the optical frequency ω_0 , and $\delta\gamma(t)$ and $\delta\psi(t)$ have been neglected. The variance ΔY^2 ($Y = X_{\phi=\pi/2}$) is given by a similar expression with γ replaced by $-\gamma$.

For a single-input cavity ($\kappa_2 = 0$), and for $\psi = 0$, the product $16\Delta X^2\Delta Y^2$ reduces to unity, corresponding to a minimum uncertainty state. In general, this condition is no more satisfied for double-ended cavities or non-zero detuning or lossy crystals. Then, it is worth characterizing the OPO output at the sampled frequency ω by means of the adimensional parameters:

$$\begin{aligned} n_{th} &= 2 \left(\sqrt{\Delta X^2 \Delta Y^2} - \frac{1}{4} \right) \\ n_{sq} &= \frac{1}{4} \left(\sqrt{\frac{\Delta X^2}{\Delta Y^2}} + \sqrt{\frac{\Delta Y^2}{\Delta X^2}} - 2 \right), \end{aligned} \quad (3)$$

representing the average number of thermal and squeezed photons, respectively. They measure the deviation of the actual state from the minimum uncertainty one and its effective squeezing. In particular, the mean total photon number is given by:

$$N_{tot} = n_{sq} + n_{th} + 2n_{sq}n_{th}, \quad (4)$$

while the variance of the generic quadrature X_ϕ reads:

$$\Delta X_\phi^2 = \frac{(2n_{th} + 1)}{4} \left(1 + 2n_{sq} + 2\sqrt{(1 + n_{sq})n_{sq}} \cos 2\phi \right). \quad (5)$$

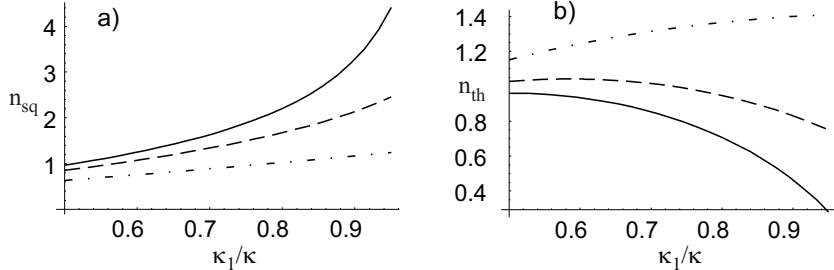


Figure 2. n_{sq} (a) and n_{th} (b) vs. coupling efficiency κ_1/κ at half of the threshold power ($\mathcal{E} = 0.5$) for $\omega = 0$. The curves refer to three different detunings $\psi = 0.0, 0.1, 0.2$ (full, dashed and dot-dashed lines).

The photon numbers n_{th} and n_{sq} depend on the frequency offset ω and on the OPO parameters, namely, distance from the threshold (\mathcal{E}), escape efficiency (κ_1/κ), and cavity detuning (ψ). In Figs. 2-a and 2-b n_{sq} and n_{th} as functions of the ratio κ_1/κ and for three different detunings ($\psi = 0.0, 0.1, 0.2$) have been plotted (OPO gain one-half of the threshold $\mathcal{E} = 0.5$ and $\omega = 0$). The detuning plays a more significant role in proximity of $\kappa_1/\kappa \simeq 1$, that is for a single-ended cavity configuration.

Since these states have been obtained by neglecting the time-dependent part of both gain and detuning, they share the Gaussian statistics of the driving fields $a_{1,2}^{in}$. They can be imagined as obtained by squeezing a thermal state $\nu = (n_{th} + 1)^{-1} [n_{th}/(n_{th} + 1)]^{a^{in}}$,

with n_{th} the number of thermal photons (see Eq.(3-a)), whose actual temperature is not necessarily coincident with the local one. As a consequence the density matrix is:

$$\varrho = S(\zeta)\nu S^\dagger(\zeta), \quad (6)$$

where $S(\zeta) = \exp\{\frac{1}{2}\zeta a^\dagger a - \frac{1}{2}\zeta^* a^2\}$ is the squeezing operator ($n_{sq} = \sinh^2 |\zeta|$) [9, 10].

These STV states are described by a Gaussian Wigner function centered at the origin:

$$\begin{aligned} W(\alpha) &= \frac{1}{2\pi\sqrt{\Delta X^2 \Delta Y^2}} \exp\left(-\frac{\Re[\alpha]^2}{2\Delta X^2} - \frac{\Im[\alpha]^2}{2\Delta Y^2}\right) \\ &= \frac{2}{\pi} \int P(\beta) \exp(-2|\alpha - \beta|^2) d^2\beta, \end{aligned}$$

with $P(\beta)$ the corresponding P-representation:

$$P(\beta) = \frac{1}{2\pi\sqrt{(\Delta X^2 - \frac{1}{4})(\Delta Y^2 - \frac{1}{4})}} \exp\left(-\frac{\Re[\beta]^2}{2(\Delta X^2 - \frac{1}{4})} - \frac{\Im[\beta]^2}{2(\Delta Y^2 - \frac{1}{4})}\right).$$

After propagation through a medium of transmittivity T the density matrix

$$\varrho = \int P(\alpha) |\alpha\rangle\langle\alpha| d^2\alpha$$

modifies as

$$\varrho_T = \int P(\alpha) \left| \sqrt{T}\alpha \right\rangle \left\langle \sqrt{T}\alpha \right| d^2\alpha = \int P_T(\alpha) |\alpha\rangle\langle\alpha| d^2\alpha,$$

with

$$\begin{aligned} P_T(\alpha) &= \frac{1}{T} P\left(\frac{\alpha}{\sqrt{T}}\right) \\ &= \frac{1}{2\pi\sqrt{(\Delta X_T^2 - \frac{1}{4})(\Delta Y_T^2 - \frac{1}{4})}} \exp\left(-\frac{\Re[\alpha]^2}{2(\Delta X_T^2 - \frac{1}{4})} - \frac{\Im[\alpha]^2}{2(\Delta Y_T^2 - \frac{1}{4})}\right), \end{aligned}$$

and

$$\Delta X_T^2 - \frac{1}{4} = T \left(\Delta X^2 - \frac{1}{4} \right).$$

$\Delta X^2 - \frac{1}{4}$ is the deviation of the actual STV variance from the vacuum state case (shot-noise). A similar expression is found for ΔY_T^2 .

In principle, in the absence of multiple reflections within the sample, the transmittivity T is given by $T = T_1 T_{slab} T_2$, where T_1 and T_2 are the Fresnel transmission coefficients at the input and output faces of the sample respectively and T_{slab} is the sample internal transmittivity.

Next, introducing the subfixes 0 and T for labelling up- and down-stream quantities, respectively, for a generic quadrature X_ϕ the variance transforms as:

$$\Delta X_{\phi,T}^2 - \frac{1}{4} = T \left(\Delta X_{\phi,0}^2 - \frac{1}{4} \right). \quad (7)$$

	A	B	$A^{(QHT)}$	$B^{(QHT)}$
N_{tot}	0	1	$-0,05 \pm 0,07$	$1,1 \pm 0,1$
n_{th}	0.12	0.89	0.07 ± 0.05	0.85 ± 0.07
n_{sq}	-0.12	1.14	-0.16 ± 0.05	1.14 ± 0.07

Table 1. Coefficients A and B computed by Eqs.(10,12) (left) and experimental ones measured by QHT (right).

Accordingly, T can be obtained by measuring the up- and down-stream quadrature variances:

$$T = \frac{\Delta X_{\phi,T}^2 - \frac{1}{4}}{\Delta X_{\phi,0}^2 - \frac{1}{4}}. \quad (8)$$

This relation suggests a simple way to measure T through the deviations of a generic quadrature from the vacuum noise level.

By means of Eqs.(5) and (8), T can be also expressed as:

$$T = \frac{(2n_{th,T} + 1) \left(1 + 2n_{sq,T} + 2\sqrt{(1 + n_{sq,T}) n_{sq,T}} \cos 2\phi \right) - 1}{(2n_{th,0} + 1) \left(1 + 2n_{sq,0} + 2\sqrt{(1 + n_{sq,0}) n_{sq,0}} \cos 2\phi \right) - 1}. \quad (9)$$

On the other hand, N_{tot} transforms proportionally to T as for a classical field:

$$N_{tot,T} = T N_{tot,0}. \quad (10)$$

Using Eq.(4) in the above expression and combining it with Eq.(9) $n_{th,T}$ and $n_{sq,T}$ can be expressed in terms of T and of the initial values $n_{th,0}$ and $n_{sq,0}$:

$$\begin{aligned} 2n_{th,T} + 1 &= \sqrt{[1 - T + T(1 + 2n_{th,0})(1 + 2n_{sq,0})]^2 - \left[2T(1 + 2n_{th,0})\sqrt{(1 + n_{sq,0}) n_{sq,0}} \right]^2} \\ 2n_{sq,T} + 1 &= \frac{1 - T + T(2n_{th,0} + 1)(1 + 2n_{sq,0})}{2n_{th,T} + 1}. \end{aligned} \quad (11)$$

For the STV state used in the test discussed in Section 4 ($n_{th,0} = 0.55$ and $n_{sq,0} = 0.11$) $n_{th,T}$ and $n_{sq,T}$ are practically linear in T , that is:

$$\begin{aligned} \frac{n_{th,T}}{n_{th,0}} &= A_{th} + B_{th}T \\ \frac{n_{sq,T}}{n_{sq,0}} &= A_{sq} + B_{sq}T. \end{aligned} \quad (12)$$

In Table 1 the coefficients calculated by linearizing Eqs.(11) have been reported (first two columns) together with those obtained experimentally (last two columns). For the sake of completeness the measured ratio $N_{tot,T}/N_{tot,0}$ has been reported as well, in order to evidenziate the agreement with the theoretical value of Eq.(10).

In the measurements discussed below, T was determined through a direct measurement of the parameters n_{th} and n_{sq} by QHT technique based on pattern functions.

In conclusion, it is worth remarking that the above expressions of T are valid for Gaussian field quadratures. A Gaussian statistics follows from the assumption of time independent gain and detuning of the OPO. In Section 4 the correctness of this assumption will be discussed for the used OPO by measuring the deviations from the Gaussian statistics by means of the kurtosis parameter K_ϕ , vanishing for the Gaussian case, defined as:

$$K_\phi = \frac{\overline{\Delta X_\phi^4}}{(\overline{\Delta X_\phi^2})^2} - 3, \quad (13)$$

$\overline{\Delta X_\phi^4}$ being the fourth order moment of X_ϕ .

3. Accuracy

The limit of the uncertainty on the estimate of T expressed by Eq.(8) depends on the confidence interval $\delta [\Delta X_\phi^2]$ in the measurement of ΔX_ϕ^2 :

$$\frac{\delta T}{T} = \frac{1}{|\Delta X_{\phi,0}^2 - \frac{1}{4}|} \sqrt{\frac{\delta [\Delta X_{\phi,T}^2]^2}{T^2} + \delta [\Delta X_{\phi,0}^2]^2}. \quad (14)$$

Since

$$\delta [\Delta X_\phi^2] = \sqrt{\frac{2}{N}} \Delta X_\phi^2,$$

with N the number of acquired data, the relative error on T is given by:

$$\frac{\delta T}{T} = \sqrt{\frac{2}{N} \frac{1}{|\Delta X_{\phi,0}^2 - \frac{1}{4}|} \sqrt{\frac{1}{16} \left(1 - \frac{1}{T}\right)^2 + \frac{1}{2} \left|\Delta X_{\phi,0}^2 - \frac{1}{4}\right| \left(\frac{1}{T} + 3 + 4 \left|\Delta X_{\phi,0}^2 - \frac{1}{4}\right|\right)}}. \quad (15)$$

This expression gives, for a given T , the relative error as a function of N and $\Delta X_{\phi,0}^2$ which in turns depends on the OPO working condition, namely, distance from the threshold (\mathcal{E}), escape efficiency (κ_1/κ), and cavity detuning (ψ). On the other hand, the total number of photons N_{ph} hitting the sample during the measurement is:

$$N_{ph} = N_{tot} N \kappa \tau_s, \quad (16)$$

with τ_s^{-1} the sampling rate and N_{tot} given by Eq.(4).

In Fig. 3-a $\frac{\delta T}{T} \sqrt{\frac{N}{2}}$ (see Eq. 15)) has been plotted as a function of the transmittivity T for $\omega = \psi = 0$, $\mathcal{E} = 0.5$, and three different escape efficiencies ($\kappa_1/\kappa = 0.5, 0.75, 1$). The relative error increases for T approaching zero. Fig.3-b gives the photon dose N_{ph} (Eq. (16)) necessary to obtain a relative error $\frac{\delta T}{T} = 0.01$ for the parameters of Fig.3-a and $\kappa \tau_s = 6$. The plot evidentiates the increase of N_{ph} by more than an order of magnitude for T less than 0.01.

Instead of keeping ϕ constant during the acquisition of the N samples, the angle can be varied uniformly in the interval $0 \leq \phi \leq 2\pi$. The ensemble so obtained

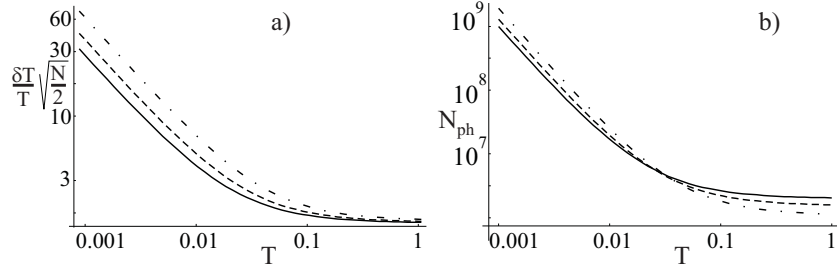


Figure 3. (a) Relative error $\frac{\delta T}{T} \sqrt{\frac{N}{2}}$ (Eq.(15)) and (b) number N_{ph} of photons hitting the sample for $\frac{\delta T}{T} = 0.01$ (Eq.(16) and $\kappa\tau_s = 6$) vs. transmittivity T . The plots refer to $\omega = \psi = 0$, at half the threshold ($\mathcal{E} = 0.5$) and $\kappa_1/\kappa = 0.5, 0.75, 1$ (dot-dashed, dashed and full lines).

can be processed by means of QHT [11] for obtaining the field Wigner function. The tomographic processing can be based on the so-called pattern function method, consisting in averaging the pattern function $R_\eta[\hat{O}](X_{\theta_j}, \theta_j)$ relative to an assigned operator \hat{O} , and having for argument the j -th realization X_{θ_j} of \hat{X}_θ for the LO phase θ_j ,

$$\langle \hat{O} \rangle = \frac{1}{N} \sum_{j=1}^N R_\eta[\hat{O}](X_{\theta_j}, \theta_j) = \overline{R_\eta[\hat{O}]}. \quad (17)$$

The suffix "η" indicates the dependence of the pattern function on the homodyne efficiency η .

For the operator $\hat{O} = \Delta X_\phi^2$ the confidence interval provided by this method reads

$$\delta_{QHT} [\Delta X_\phi^2] = \frac{1}{\sqrt{N}} \sqrt{\overline{\Delta R^2} [\Delta X_\phi^2]}, \quad (18)$$

with $\overline{\Delta R^2} [\hat{O}] = \overline{R_\eta^2[\hat{O}]} - \overline{R_\eta[\hat{O}]}^2$. Consequently Eq. (14) is still valid with $\delta [\Delta X_\phi^2]$ replaced by $\delta_{QHT} [\Delta X_\phi^2]$.

Next, taking into account the analytic expressions of $R_\eta^2[\Delta X_\phi^2]$ and $R_\eta[\Delta X_\phi^2]$ [12], it can be shown that:

$$\overline{\Delta R^2} [\Delta \hat{X}_\phi^2] = C_0 + C_1 \cos(2\phi) + C_2 \cos(4\phi), \quad (19)$$

with the coefficients C_0 , C_1 and C_2 given in Appendix. For the variances $\Delta X^2, \Delta Y^2$ relative to OPO devices similar to that used in the experimental test, $\delta_{QHT} [\Delta X_\phi^2]$ differs from $\delta [\Delta X_\phi^2]$ only by some percents. This means that collecting N samples in the interval $(0, 2\pi)$ reduces the accuracy with respect to the constant phase case by only a few percent.

Conventional measurements of T using coherent CW probe beams and the radiation power, P , as observable, are in some way corrupted by the detector noise equivalent power (NEP), and the measurement error reads:

$$\delta P = \sqrt{\hbar\omega_0 B P} + NEP, \quad (20)$$

with ω_0 the radiation frequency, and B the detection bandwidth.

Measuring T as the ratio P_T/P_0 of the power down- and up-stream the sample the relative error is:

$$\frac{\delta T}{T} = \frac{1}{SNR} \sqrt{\frac{1}{T^2} \left(1 + \sqrt{\frac{\hbar\omega_0 B}{NEP} \frac{SNR T}{N}} \right)^2 + \left(1 + \sqrt{\frac{\hbar\omega_0 B}{NEP} \frac{SNR}{N}} \right)^2}, \quad (21)$$

with $SNR = P_0/NEP$ and N the number of data.

The total number of photons (see Eq. (16)) passing through the sample during the measurement interval is now given by

$$N_{ph} = SNR \frac{NEP}{\hbar\omega_0} N\tau_s \quad (22)$$

so that, the factor $\frac{\hbar\omega_0 B}{NEP N}$ in Eq. (21) can be replaced by $\frac{SNR B\tau_s}{N_{ph}}$ (with $B\tau_s > 1$). Then the ratio $\frac{B\tau_s}{N_{ph}}$ is a function of $\frac{\delta T}{T}$, T and SNR . Using for SNR the limiting value

$$SNR \geq \frac{T}{\delta T} \sqrt{\frac{1}{T^2} + 1},$$

the plot of Fig. 4 representing N_{ph} vs. T for $\frac{\delta T}{T} = 0.01$ and $B\tau_s = 10$ has been obtained. Comparing it with Fig. 3-b it appears evident the much lower photon dose required by the present method.

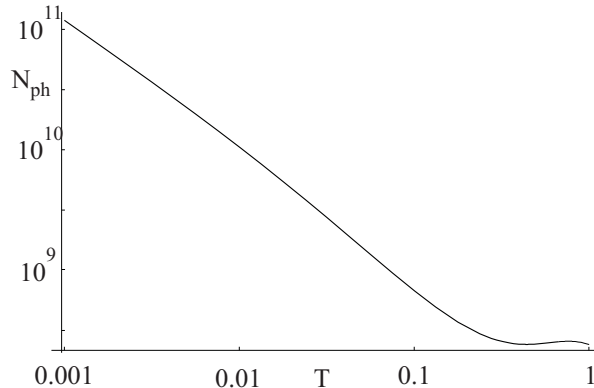


Figure 4. Photon dose passing through the sample (N_{ph}) vs. T in case of standard transmission measurements. The curve refer to $B\tau_s = 10$ and $\frac{\delta T}{T} = 0.01$.

In case a coherent beam (a_α) is mixed with a squeezed thermal vacuum one (a_{STV}), as in Ref. [3], the total field is described by:

$$a_{tot} = e^{i\theta} a_{STV} + a_\alpha,$$

with θ their locked phase difference.

It can be shown that the addition of the squeezed component modifies slightly Eq. (20) with B replaced by

$$B_{eff} = B \left(1 + n_{sq} + n_{th} + 2n_{sq}n_{th} + \sqrt{(1 + n_{sq}) n_{sq}} \cos 2\theta \right).$$

For $\cos 2\theta = -1$ and $\sqrt{(1 + n_{sq}) n_{sq}} > n_{sq} + n_{th} + 2n_{sq}n_{th}$ the squeezed vacuum component reduces the effective detector bandwidth. The reduction of B (typically $B_{eff} \gtrsim .5B$) implies a proportional decrease of N_{ph} for assigned $\frac{\delta T}{T}$ and T .

4. The experiment

The reliability and accuracy of the method were tested with a sample of variable transmittivity. The T values obtained via QHT were compared to those measured, with an accuracy of 10^{-4} , with standard techniques employing 1 mW coherent beam at $\lambda = 1064$ nm. A schematic of the experimental set-up is shown in Fig. 1.

STV states were generated by a degenerate type-I OPO and characterized by a homodyne detector, both described in details in Ref. [13]. In the present case, cavity mirrors were adjusted in such a way as to have a cavity linewidth of 15 MHz.

The OPO output was propagated through a variable neutral density filter, which changes T without introducing misalignment, and keeping homodyne visibility at a constant value. The transmittivity T was varied between 0.45 and 1 in discrete steps. The beam passing through the non-absorbing zone ($T = 1$) of the filter was used as a reference state. The field leaving the absorber was sent to an homodyne detector with an overall efficiency of $\eta = 0.88 \pm 0.02$. The average electrical signal level at the homodyne output was 15 dB higher than the electronic noise.

Tomographic data were acquired by sampling the homodyne signal. To avoid any effect of the laser technical noise on the measurement, data sampling was performed by mixing the homodyne current with a sinusoidal signal of frequency $\Omega = 5$ MHz. Then, the resulting current was low-pass filtered, with a cut-off frequency of 2.5 MHz, and 10^6 samples were collected with at 2.5 Msample/s ($\tau_s = 400$ ns) in order to pick-up statistically independent data.

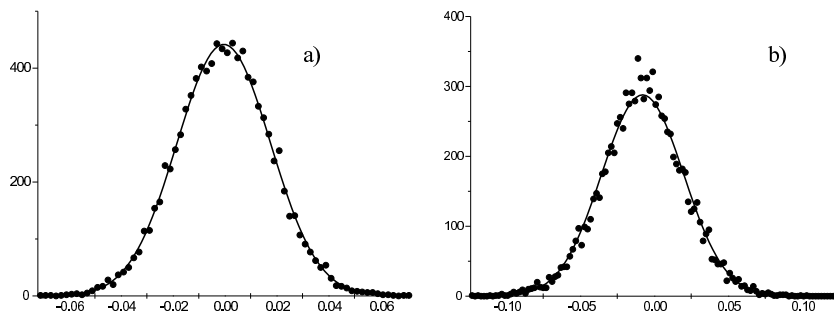


Figure 5. Distribution of X values measured for $\mathcal{E} = 0.5$ a) and 0.95 b). The kurtosis K_0 (Eq. (13)) is respectively equal to 0.005 and 0.5. Full lines represent Gaussian with the same mean and variance.

Fixing $\mathcal{E} = 0.50$ the reference STV state had $N_{tot,0} = 0.79 \pm 0.06$, $n_{th,0} = 0.55 \pm 0.02$ and $n_{sq,0} = 0.11 \pm 0.01$, corresponding to a photon flux of 10^7 s $^{-1}$. For this state it resulted $K_\phi \lesssim 0.01$ (see Fig. 5-a and Eq.(13)) for any ϕ , thus indicating that the corresponding quadrature statistics was very close to the Gaussian one.

In order to reduce the influence of residual fluctuations of the STV state, each experimental point was averaged over multiple (~ 5) tomographic acquisitions. In the present conditions the QHT error was negligible with respect to the standard deviations of the STV state parameters.

To assess the robustness of the method, the transmittivity, T_{QHT} , obtained by tomographic reconstruction was compared with the corresponding value, T_{st} , provided by standard intensity measurements.

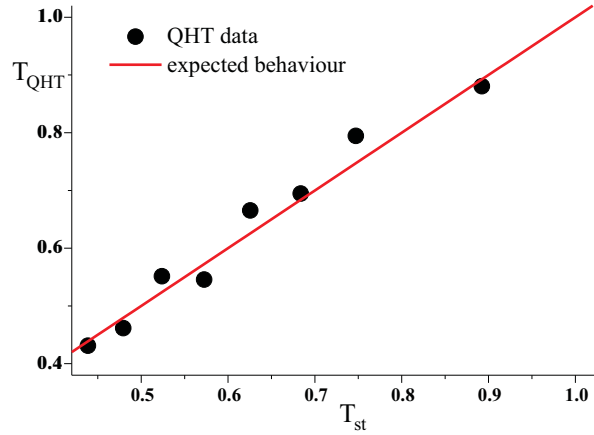


Figure 6. T_{QHT} vs. T_{st} . Experimental points are plotted together with the expected behaviour of Eq. (10) (straight line).

In Fig. 6, $T_{QHT} = N_{tot,T}/N_{tot,0}$ (see Eq.(10)) was plotted vs. T_{st} together with the expected behavior $T_{QHT} = T_{st}$ (straight line). A linear regression of the data with $T_{QHT} = A_{tot}^{(QHT)} + B_{tot}^{(QHT)}T_{st}$, gave $A_{tot}^{(QHT)} = -0.05 \pm 0.07$ and $B_{tot}^{(QHT)} = 1.1 \pm 0.1$ in good agreement with the expected values of $A_{tot} = 0$ and $B_{tot} = 1$ respectively.

In order to estimate T_{QHT} through other quantities, the measured value of $n_{sq,T}/n_{sq,0}$ versus T_{st} was plotted in Fig. 7 together with the linear approximation of Eq. (12-b). Linear regression on experimental data gave $A_{sq}^{(QHT)} = -0.16 \pm 0.05$ and $B_{sq}^{(QHT)} = 1.14 \pm 0.07$, values in good agreement with $A_{sq} = -0.12$, $B_{sq} = 1.14$.

Each experimental point of Fig. 7 represents an average value obtained over multiple acquisitions. In the inset the different values of T_{QHT} , corresponding to four acquisitions at $T_{st} = 0.64$ are reported. The bar indicates the quantum limit error, calculated by using Eq. (15). As it can be seen, all the points are spread over a range comparable to the quantum limit.

In Fig. 8 the shadowed area represents the quantum limit for the accuracy vs. T (see Eq.(15)) for the present experimental conditions and $N = 10^4$. The accuracy width is almost constant in the tested range of T while it deteriorates for low transmittivity, as expected.

Finally, an identical behavior was observed for $n_{th,T}/n_{th,0}$ (not plotted) resulting in $A_{th}^{(QHT)} = 0.07 \pm 0.05$, $B_{th}^{(QHT)} = 0.85 \pm 0.07$ ($A_{th} = 0.12$, $B_{th} = 0.89$).

A summary of the experimental findings is reported in Table 1.

The photon flux at the OPO output $F = N_{tot}/\tau$, with τ the cavity photon lifetime,

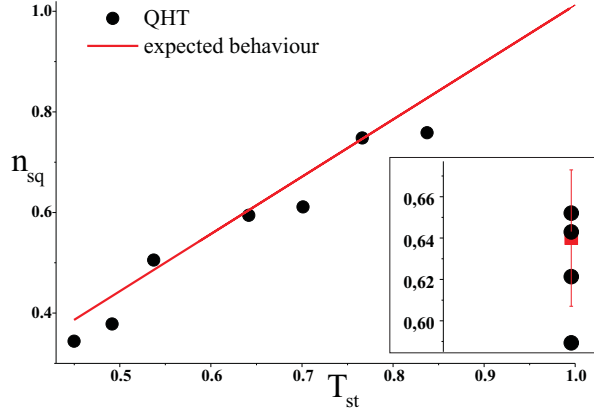


Figure 7. $n_{sq,T}$ vs. T_{st} . Experimental points are compared with Eq.(12b). The points in the inset are relative to four measurements for an attenuator transmittivity equal to 0.64 while the error bar has been calculated by using Eq. (15).

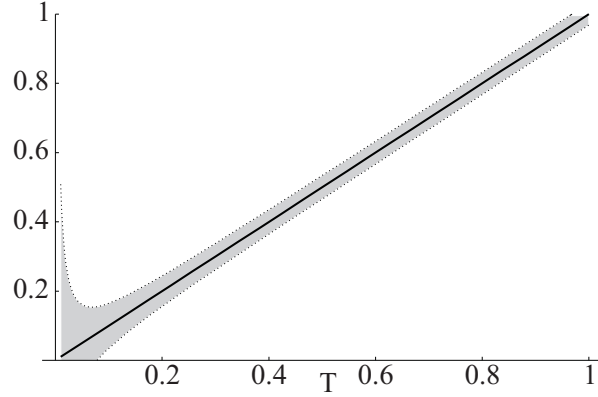


Figure 8. Quantum limit (shadowed area) of the relative error on T for the experimental case discussed in the text and $N = 10^4$.

was less than 10^7 s $^{-1}$, for $N_{tot} \lesssim 0.7$ and $\tau \approx 6.6 \times 10^{-8}$, corresponding to an optical power $\lesssim 4.2$ pW. The method was tested for different input states, by varying \mathcal{E} and hence the photon flux by showing a good reliability down to a photon flux $F \sim 5 \times 10^6$ s $^{-1}$ (i.e. ~ 2.2 pW and $N_{tot,0} = 0.37$).

With $N = 10^6$ $\delta_{QHT} [\Delta X^2] \sim 1.3 \times 10^{-3}$ and $\delta_{QHT} [\Delta Y^2] \sim 0.8 \times 10^{-3}$ corresponding to $\delta T/T \sim 0.0024$ and ~ 0.056 for $T = 1$. These QHT estimates were slightly less accurate than those one could obtain by concentrating $N/2$ data on X and $N/2$ on Y quadratures and computing their variances.

5. Conclusions

A scheme for measuring the optical transmittivity of a sample by using squeezed vacuum radiation has been illustrated. Main advantage of this method is a number of photons hitting the sample during the measurement some orders of magnitude smaller than that relative to standard techniques based on intensity measurements of coherent beams.

The core of the method consists in the measurement of the variance ΔX_ϕ^2 of a

generic quadrature of a squeezed vacuum field, generated by a below threshold OPO and passing through the sample under investigation. The quadrature is measured by a homodyne detector. In the simplest implementation ΔX_ϕ^2 is obtained by averaging the squared samples X_ϕ relative to a constant phase ϕ . In the test described in the paper X_ϕ has been obtained by scanning the interval $\phi \in (0, 2\pi)$. This approach has been preferred since it provides a complete reconstruction of the squeezed vacuum Wigner function.

Essential to this scheme is the assumption of Gaussian statistics for the squeezed vacuum field. This property has been checked on the recorded samples relative to a given phase and confirmed by the field Wigner function.

The accuracy of this method has been compared with that based on absorption of coherent beams (with and without a squeezed vacuum component) as a function of sample transmittivity, number of data and detection bandwidth. In the case the number of photons interacting with the sample during the measurement is an important parameter, the proposed method is the most accurate.

The experimental tests have shown that, for photon fluxes of the order of few pW (at 1064 nm), the accuracy is of the order of the quantum limit, that is the method does not suffer substantially from other technical noise sources

Acknowledgments

This work has been supported by MIUR through the project PRIN-2005024254.

References

- [1] Carlton M. Caves, "Quantum-mechanical noise in an interferometer", *Phys. Rev. D* **23**, 1693-1708 (1981);
- [2] P. Grangier, R. E. Slusher, B. Yurke, and A. LaPorta "Squeezed-lightenhanced polarization interferometer" *Phys. Rev. Lett.* **59**, 2153-2156 (1987);
- [3] E. S. Polzik, J. Carri, and H. J. Kimble, "Spectroscopy with squeezed light ". *Phys. Rev. Lett.* **68**, 3020-3023 (1992);
- [4] A. S. Lane, M. D. Reid and D. F. Walls "Quantum analysis of intensity fluctuations in the nondegenerate parametric oscillator" *Phys. Rev. A* **38**, 788-799 (1988);
- [5] P. R. Tapster, S. F. Seward, and J. G. Rarity "Sub-shot-noise measurement of modulated absorption using parametric down-conversion" *Phys. Rev. A* **44**, 3266-3269 (1991);
- [6] C. D. Nabors and R. M. Shelby, "Two-color squeezing and sub-shot-noise signal recovery in doubly resonant optical parametric oscillators" *Phys. Rev. A* **42**, 556-559 (1990);
- [7] J.J. Snyder, E.Giacobino, C.Fabre, A.Heidmann and M.Ducloy "Sub shot noise measurements using the beat note between quantum-correlated photon beams", *JOSA B* **7** 2132 (1990);
- [8] A. Porzio, C. Altucci, M. Autiero, A. Chiummo, C. de Lisio, and S. Solimeno, "Tunable twin beams generated by a type-I LNB OPO", *Appl. Phys. B* **73**, 763–766, (2001);
- [9] P. Marian, "Higher-order squeezing and photon statistics for squeezed thermal states", *Phys. Rev. A* **45**, 2044–2051 (1992);
- [10] V. V. Dodonov, O. V. Manko, V. I. Manko, "Photon distribution for one-mode mixed light with a generic Gaussian Wigner function", *Phys. Rev. A*, **49**, 2993 (1994);

- [11] See for example: "Quantum states estimation", M. G. A. Paris and J. Řeháček Eds., Lect. Not. Phys. **649** (Springer, Heidelberg, 2004)
- [12] G. M. D'Ariano, M. G. A. Paris, and M. F. Sacchi, "Quantum Tomography", Advances in Imaging and Electron Physics **128**, 205–308 (2003);
- [13] V. D'Auria, A. Chiummo, M. De Laurentis, A. Porzio, S. Solimeno, and M. G. Paris, "Tomographic characterization of OPO sources close to threshold," Opt.Express **13**, 948-956 (2005).

Appendix

The coefficients C_0 , C_1 and C_2 of Eq. (19) are given by:

$$C_0 = \frac{1}{4} \left[\frac{27}{2} (\Delta X^4 + \Delta Y^4) + 9\Delta X^2 \Delta Y^2 + \left(1 - \frac{3}{\eta}\right) (\Delta X^2 + \Delta Y^2) + \frac{1}{4} \left(\frac{3}{\eta^2} - \frac{2}{\eta} + 1 \right) \right]$$

$$C_1 = \frac{1}{2} (\Delta X^2 - \Delta Y^2) [3 (\Delta X^2 + \Delta Y^2) - 1]$$

$$C_2 = \frac{3}{8} (\Delta X^2 - \Delta Y^2)^2 .$$